Published in final edited form as:
Gen Relativ Gravit. 2018 ; 50(6): . doi:10.1007/s10714-018-2373-5.

The Collisional Penrose Process

Jeremy D. Schnittman
NASA GSFC, 8800 Greenbelt Road, mail code 663, Greenbelt, MD 20771

Abstract

Shortly after the discovery of the Kerr metric in 1963, it was realized that a region existed outside of the black hole's event horizon where no time-like observer could remain stationary. In 1969, Roger Penrose showed that particles within this ergosphere region could possess negative energy, as measured by an observer at infinity. When captured by the horizon, these negative energy particles essentially extract mass and angular momentum from the black hole. While the decay of a single particle within the ergosphere is not a particularly efficient means of energy extraction, the *collision* of multiple particles can reach arbitrarily high center-of-mass energy in the limit of extremal black hole spin. The resulting particles can escape with high efficiency, potentially erving as a probe of high-energy particle physics as well as general relativity. In this paper, we briefly review the history of the field and highlight a specific astrophysical application of the collisional Penrose process: the potential to enhance annihilation of dark matter particles in the vicinity of a supermassive black hole.

Keywords

black holes; ergosphere; Kerr metric

1 Introduction

We begin with a brief overview of the Kerr metric for spinning, stationary black holes [1]. By far the most convenient, and thus most common form of the Kerr metric is the form derived by Boyer and Lindquist [2]. In standard spherical coordinates (t, r, θ, ϕ) the metric is given by

$$g_{\mu\nu} = \begin{pmatrix} -\alpha^2 + \omega^2\varpi^2 & 0 & 0 & -\omega\varpi^2 \\ 0 & \rho^2/\Delta & 0 & 0 \\ 0 & 0 & \rho^2 & 0 \\ -\omega\varpi^2 & 0 & 0 & \varpi^2 \end{pmatrix}. \quad (1)$$

This allows for a relatively simple form for the inverse metric:

jeremy.schnittman@nasa.gov.

$$g^{\mu\nu} = \begin{pmatrix} -1/\alpha^2 & 0 & 0 & -\omega/\alpha^2 \\ 0 & \Delta/\rho^2 & 0 & 0 \\ 0 & 0 & 1/\rho^2 & 0 \\ -\omega/\alpha^2 & 0 & 0 & 1/\varpi^2 - \omega^2/\alpha^2 \end{pmatrix}. \tag{2}$$

In geometrized units with $G = c = 1$, we have defined the following terms

$$\rho^2 \equiv r^2 + a^2\cos^2\theta \tag{3a}$$

$$\Delta \equiv r^2 - 2Mr + a^2 \tag{3b}$$

$$\alpha^2 \equiv \frac{\rho^2\Delta}{\rho^2\Delta + 2Mr\left(a^2 + r^2\right)} \tag{3c}$$

$$\omega \equiv \frac{2Mra}{\rho^2\Delta + 2Mr\left(a^2 + r^2\right)} \tag{3d}$$

$$\varpi^2 \equiv \left[\frac{\rho^2\Delta + 2Mr\left(a^2 + r^2\right)}{\rho^2}\right]\sin^2\theta\,. \tag{3e}$$

It is also convenient to define a dimensionless spin parameter $a_* = a/M$ with $0 \le a_* \le 1$. Black holes with $a_* = 1$ are called *maximally spinning* or *extremal*.

In these coordinates, the event horizon is located on the surface defined by $\Delta(r) = 0$, giving both an inner and outer horizon:

$$r_\pm = M \pm M\sqrt{1 - a_*^2}\,. \tag{4}$$

The outer horizon r_+ is generally referred to as the event horizon, while r_- is also known as the Cauchy horizon.

Consider a coordinate-stationary observer with 4-velocity $u^\mu = (u^t, 0, 0, 0)$. For the observer to have a time-like (i.e. physical) trajectory, we require $g_{tt}u^tu^t < 0$, or alternatively:

$$g_{tt} = -\left(1 - \frac{2Mr}{r^2 + a^2\cos^2\theta}\right) < 0, \tag{5}$$

or

$$r > M + M\sqrt{1 - a_*^2\cos^2\theta}\,. \tag{6}$$

This implies that there is a region outside of r_+ where no stationary observer can exist. This space is called the *ergosphere,* and is bounded by the surface defined by $r_{\rm E} = M + M\sqrt{1 - a_*^2\cos^2\theta}$. While the volume of the ergosphere is greatest for highly-spinning black holes, it exists for any black hole with $r_E > r_+$, which is satisfied whenever $a_* > 0$. This is expected to be the case for all astrophysical black holes.

In 1969, Roger Penrose realized that reactions taking place within the ergosphere could result in particles with negative energy [3]. What does it mean for a particle to have negative energy? Locally, any observer with 4-velocity u^μ measures the energy of a particle with momentum p_μ with a simple inner product: $E_{\rm obs} = -p_\mu u^\mu$. An observer at rest at infinity has $u^\mu = [1, 0, 0, 0]$ so we can define the "energy at infinity" of a particle to be $E_\infty = -p_t$. For stationary spacetimes, p_t is an integral of motion, so a particle's energy at infinity is conserved. Thus it is possible for a particle to have positive energy, as measured by an observer in the ergosphere, yet still have $p_t > 0$. Such a particle simply would not be able to escape the ergosphere, and would rapidly be captured by the black hole (all the while maintaining Christodoulou's limits [4] on the black hole mass and spin).

Shortly after Penrose's 1969 paper, some authors proposed that this remarkable feature of spinning black holes might be responsible for the high-energy radiation seen from some active galaxies. But a careful analysis by Bardeen et al. [5] and Wald [6] showed that it was impossible to attain relativistic energies due to the Penrose process alone. A particle would have to emit a daughter particle with energy a significant fraction of the original particle's rest mass in order for the surviving particle to itself reach relativistic velocities. And in this case, while the escaping particle may in fact be moving near the speed of light, it can only do so by sacrificing its own rest mass energy.

Quantitatively, Wald [6] showed that a particle with initial energy E and mass m can decay into a particle with energy E' and m' in the range

$$\gamma\frac{E}{m} - \gamma v\left(\frac{E^2}{m^2} + 1\right)^{1/2} \le \frac{E'}{m'} \le \gamma\frac{E}{m} + \gamma v\left(\frac{E^2}{m^2} + 1\right)^{1/2}. \tag{7}$$

Here, γ is the Lorentz factor of the daughter particle in the original particle's rest frame. For a particle falling in from rest at infinity ($E/m = 1$) and breaking into two equal-mass particles with mass m' in the ergosphere, we see that the lower energy limit can be negative when $v > 2^{-1/2}$. This is equivalent to two daughter particles each with rest mass of only 35% of the original particle. In the limit of 2-photon decay, the upper limit is given by $E' \le E\frac{1+\sqrt{2}}{2}$, corresponding to an efficiency of ~ 121%.

Here we should note that our definition of efficiency differs slightly from some previous works. For example, Piran & Shaham [7] define the efficiency of the Penrose process by

$$\eta_{\rm P-S} \equiv \frac{E_{\rm esc} - E_{\rm in}}{E_{\rm in}} = \frac{-E_{\rm cap}}{E_{\rm in}}, \tag{8}$$

where the incoming particle has energy $E_{\rm in}$, the escaping particle $E_{\rm esc}$, and the particle captured by the black hole has $E_{\rm cap}$, which is taken to be negative for the Penrose process. In an attempt to distinguish between the exotic nature of the Penrose process and more conventional physical processes, we use a definition of efficiency that compares total energy out with total energy in:

$$\eta \equiv \frac{E_{\rm esc}}{E_{\rm in}}, \tag{9}$$

which will have values exceeding 100% for the Penrose process.

Now, 121% efficiency in converting mass to energy is nothing to dismiss lightly. It far exceeds the efficiency of nuclear fusion, and even exceeds the radiative efficiency of quasars (assuming Novikov-Thorne thin accretion disks [8] and maximal spin, efficiency of 40% might be attained [9]). It is the ultimate “free lunch:” getting more energy out than you put in. Yet it still cannot explain the GeV or even TeV emission seen in blazars, or the large-scale, relativistic jets seen emerging from radio galaxies with bulk Lorentz factors of 10 or more, and this was one of the outstanding mysteries that Penrose, Wald, and others at the time were trying to solve [3, 6].

While not an obvious solution for the origin of relativistic jets, the Penrose process was seen, perhaps whimsically, as a potential and exotic source of energy for an extremely advanced civilization living around a Kerr black hole. This is shown in Figure 1, reproduced from Penrose’s original 1969 paper.

Shortly after Wald published his limit of 121%, Piran and collaborators discovered a way to attain an even higher efficiency from the Penrose process [10, 7]. The crucial point was to use more than one particle, in order to achieve a much higher center-of-mass energy in the ergosphere. This approach is known as the *Collisional Penrose Process.*

The collisional Penrose process is a great deal richer than the simple decay problem considered by Wald, where it was clear from inspection what was the geometry required for maximal efficiency. For *two* incoming particles, the range of possible values for the total energy and momentum are vastly greater. Further expanding the population of colliding particles to those with $E_0/m \neq 1$ and non-planar orbits makes the problem virtually intractable for analytic methods. However, from symmetry arguments we can limit our focus on specialized planar orbits around extremal black holes when looking for the highest efficiency reactions.

As discussed at length in [7], it is not enough for the daughter particles to have large values of energy-at-infinity, but they must also be able to escape the potential of the black hole. Following our approach in [11], we can write down an effective potential for geodesic trajectories in the equatorial plan around a Kerr black hole. From the normalization constraint $g_{\mu\nu}p^\mu p^\nu = -m^2$ we have

$$V_{\rm eff}(r) = k\frac{M}{r} + \frac{\ell^2}{2r^2} + \frac{1}{2}\left(-k - \varepsilon^2\right)\left(1 + \frac{a^2}{r^2}\right) - \frac{M}{r^3}(\ell - a\varepsilon)^2, \tag{10}$$

where ℓ and ε are the particle's specific angular momentum and energy, and $k = 0$ for photons and $k = -1$ for massive particles. For a specific choice of a, ℓ, ε, and k, we can solve for the radial turning points by setting $V_{\rm eff}(r) = 0$.

Figure 2 shows these turning points as a function of the impact parameter $b \equiv \ell/\varepsilon$ for both massless and massive particles, for maximal spin $a_* = 1$. For the massive particles we set $\varepsilon = 1$, corresponding to a particle at rest at infinity. One can visualize a massive particle incoming from the right with $b < -2(1+\sqrt{2})$ or $b > 2$, reflecting off the centrifugal potential barrier and returning back to infinity (yellow regions). Alternatively, if the impact parameter is small enough [i.e., $-2(1+\sqrt{2}) < b < 2$], the particle will get captured by the black hole. Due to frame-dragging, the cross section for capture is much greater for incoming particles with negative angular momentum [12].

For a given $\ell = p_\phi$ and $\varepsilon = -p_t$, the radial momentum p_r can be determined from the normalization condition $p_\mu p_\nu g^{\mu\nu} = k$:

$$p_r = \pm\left[g_{rr}\left(k - g^{tt}\varepsilon^2 + 2g^{t\phi}\ell\varepsilon - g^{\phi\phi}\ell^2\right)\right]^{1/2}, \tag{11}$$

and the sign of the root is chosen depending on criterion described below. The conditions described by equation (11) and Figure 2 will be essential in understanding the range of energies attainable by outgoing particles. Yet before we get to that calculation in Section 3, we will give an overview of the "BSW" effect, named after the paper in 2009 by Banados, Silk, and West [13], which revitalized interest in the field more than thirty years after the exhaustive analysis of [7].

2 Banados-Silk-West

The primary result of BSW is that, for two particles falling in from rest at infinity, in the limit of extremal spin and collisions close to the horizon, the center-of-mass energy can reach arbitrarily high levels. This effect was indeed pointed out in [7], but those authors recognized it as not particularly interesting from an astrophysical point of view. Perhaps also because of the numerical simplicity of BSW, it received a great deal of attention immediately after publication. In this section, we will first repeat the BSW calculation, and then summarize a collection of critiques about the possibility of ever reaching such energies in practice. There have also been a great number of papers focusing on BSW-type reactions, but for non-Kerr black holes. In the interest of brevity, we do not include any discussion of those results in this review, which is focused specifically on the classical collisional Penrose process.

Figure 3 is reproduced from BSW, showing a schematic picture of the incoming particles colliding near the horizon. As can be derived from equation (10) and Figure 2, the allowed

range for the impact parameter b (same as BSW l, as the energy for particles falling in from infinity is unity) is

$$-2(1+\sqrt{1+a_*}) < b < 2(1+\sqrt{1-a}). \tag{12}$$

We take our two particles $\mathbf{p}^{(1)}$ and $\mathbf{p}^{(2)}$ to have 4-momentum components $[-1, p_r^{(1,2)}, 0, \ell^{(1,2)}]$ with p_r computed as above in equation (11).

The center-of-mass energy is given by the expression

$$E_{\rm com} = \sqrt{2(1 - g^{\mu\nu} p_\mu^{(1)} p_\nu^{(2)})}. \tag{13}$$

The simplified expression from BSW is

$$E_{\rm com}^2 = \frac{2m_0^2}{r\left(r^2 - 2r + a_*^2\right)}\left[2a^2(1+r) - 2a\left(\ell^{(1)} + \ell^{(2)}\right) - \ell^{(1)}\ell^{(2)}(r-2) + 2(r-1)r^2 - \sqrt{2\left(a - \ell^{(1)}\right)^2 - \ell^{(1)2} + 2r^2}\sqrt{2\left(a - \ell^{(2)}\right)^2 - \ell^{(2)2} + 2r^2}\right] \tag{14}$$

.

Note that BSW adopts units such that the mass is taken to be unity, and thus does not appear in equation (14). The denominator in equation (14) is always zero at the horizon, so it may appear at first glance that the center-of-mass energy always diverges, regardless of black hole spin. However, from the effective potential Figure 2, one sees that only a range of allowed values for b are able to actually reach the horizon. When taking these limits for $\ell^{(1,2)}$ and taking the location of the collision to approach the horizon, one finds that the center-of-mass energy is in fact finite for non-extremal spins. The actual algebraic expression is rather cumbersome, but in Figure 4 we plot $E_{\rm com}$ for these critical orbits, assuming a collision just outside the event horizon. Note that while the energy diverges in the limit of $a_* \to 1$, it does so quite slowly, roughly as $E_{\rm com} \sim (1 - a_*)^{-1/4}$.

Equation (14) simplifies significantly for extremal black holes with $a_* = 1$, giving the center-of-mass energy at the horizon as [13]

$$E_{\rm com}^2 = 2m_0^2\left(\frac{\ell^{(2)} - 2}{\ell^{(1)} - 2} + \frac{\ell^{(2)} - 2}{\ell^{(1)} - 2}\right). \tag{15}$$

Thus if either (but not both) of the particles have the critical angular momentum of $\ell = 2$, the collisional energy diverges.

This divergence for the extremal case is closely related to the curvature structure of the horizon. It is well known that the singularity of the Kerr metric at the horizon is only a coordinate singularity for Boyer-Lindquist coordinates [14]. A whole class of coordinates exists (e.g., Kerr-Schild, Doran) that do not blow up at the horizon, and are thus useful for

calculating the trajectories of particles near or across the horizon. However, in the limit of extremal Kerr, the curvature singularity approaches the horizon at Boyer-Lindquist $r = M$ (a super-extremal black hole would have the singularity *outside* the horizon, and thus violate the cosmic censorship conjecture), and thus physical, coordinate-independent quantities such as the center-of-mass energy can diverge.

In response to BSW, Lake [15] and Gau & Zhong [16] showed that the c.o.m. energy for collisions *inside* the horizon will generically diverge even for non-extremal black holes as the particles approach the inner Cauchy horizon, which is itself outside of the curvature singularity (they all coincide with $r = M$ in the extremal limit). Along these lines, ref. [17] showed that, for black holes with $a_* > 1$ (naked singularities), infinite c.o.m. energy collisions were quite generic.

While the diverging energy is apparently mathematically possible, in the wake of BSW, numerous authors raised physical or astrophysical objections to the proposition of using Kerr black holes to probe extreme particle energies. Here we provide a brief summary of some of the more interesting objections. Please see [18] for an excellent review of the topic.

- Berti et al. [19] point out two practical problems: even in the limit of an initially extremal black hole, a single collision would deposit the mass and angular momentum of the debris particles, lowering the black hole spin far below the levels needed for Planck-scale collisions. Additionally, the critical orbits required for diverging $E_{\rm com}$ take an infinite amount of proper time to actually reach the horizon. During this time, a particle would orbit so many times that it would actually emit a significant amount of energy and angular momentum in gravitational radiation, in turn reducing the spin of the black hole. For the much more astrophysical spin limit of $a_* = 0.998$ [9], the peak energy would be a paltry 6.95 times the rest-mass energy [20].
- Jacobson & Sotiriou [21] show that the scaling of $E_{\rm com}$ is extremely weak with the spin. For near-maximal $a = 1 - \epsilon$, they find the peak energy to be $E_{\rm com} \sim 4.06\epsilon^{-1/4}$ (see Fig. 4 above). Aside from this weak scaling restriction, they also show that any energy gained by colliding near the horizon will necessarily be lost by the redshift of escaping the black hole potential.
- Harada & Kimura [20] demonstrated similar scaling for particles falling in from the inner-most stable circular orbit (ISCO). For (non-plunging) particles on ISCO orbits colliding with generic particles falling in from infinity, the peak center-of-mass energy has an even weaker scaling: $E_{\rm com} \sim 5\epsilon^{-1/6}$.
- Bejger *et al.* [22] focus on the problem of the escaping particle's energy. They agree that an arbitrary center-of-mass energy can be achieved, but like [21], point out that the reaction products lose much of their energy on the way out from the horizon, ultimately limiting the efficiency of the process to 129% for equal-mass particles falling in from infinity.

- Harada *et al.* [23] carry out a more general calculation including non-equal mass particles and Compton scattering reactions, yet mistakenly calculate an even smaller upper limit of 109% for efficiency in the BSW-type reaction.
- Ding *et al.* [24] are the first to introduce the additional limitations that will arise from a quantum theory of gravity. By including the effects of a non-commutative spacetime via a parameterized effective field theory, they show that the maximum center-of-mass energy attainable is of the order of a few thousand times the particle rest mass, but depends on the black hole mass (in quantum gravity, black holes are no longer scale invariant).
- Galajinsky [25] repeats the BSW calculation in both Boyer-Lindquist and Near-Horizon Extremal Kerr (NHEK) coordinates, and surprisingly finds two different answers for the maximum c.o.m. energy, with it diverging in the classical Boyer-Lindquist approach, but remaining finite in NHEK. This apparent paradox is likely due to the order in which various diverging limits are taken, and which values are allowed for particle trajectories, with the consensus appearing that the B-L result is correct [26].
- Patil *et al.* [27] point out that for ultra-high values for the c.o.m. energy, the critical particles must come in with such finely-tuned values of angular momentum that they take a nearly infinite amount of coordinate time to reach the horizon, or even the radius of collision necessary for Planck-scale energies. A potential way around this problem with multiple collisions was identified by Griv & Pavlov [28].
- Like Berti *et al.* [19], McCaughey [29] also questions the possibility of an extremal black hole existing in nature. In particular, he focuses on the problem of Hawking radiation combined with the Penrose process of virtual particles in the ergosphere, which have a tendency of spinning down the black hole. Unfortunately, that paper does not include a quantitative estimate of the physical spin-down rate as a function of black hole mass and spin (see below).
- Most recently, Hod [30] raised yet another problem for reaching the highest c.o.m. energies, based on Thorne's classic hoop conjecture [31]. Simply put, if you pack enough energy into a small enough area, you form a black hole. In the context of the BSW process, if this energy is in the form of the colliding particles, and they are close enough to the horizon, then the two black holes instantly merge, and the daughter particles cannot escape, regardless of their nominal energy and angular momentum.

In the process of compiling this collection of challenges to the possibility of a divergent c.o.m. energy, two other potential problems occurred to us, apparently not addressed up to this point in the literature. The first is the spin-down of the extremal black hole due to Hawking radiation [32, 33]. This effect was first explored by Page in 1976 [34], and that is still one of the clearest, most comprehensive analyses of mass and spin evolution due to Hawking radiation. One of the interesting results from [34] is that, for extremal black holes, the evolution is dominated by graviton losses, orders of magnitude greater than the

contribution of photons or neutrinos. This is perhaps not surprising, as the curvature singularity is so close to the horizon for $a_* = 1$.

Writing $a_* = J/M^2$, the expression for spin evolution due to Hawking radiation is given by

$$\begin{aligned}\frac{da_*}{dt} &= -2M^{-3}J\frac{dM}{dt} + M^{-2}\frac{dJ}{dt} = -2a_*\dot{M}/M + \dot{J}/M^2 \\ &= M^{-3}a_*[2f(a_*) - g(a_*)],\end{aligned} \tag{16}$$

where $f(a_*)$ and $g(a_*)$ are numerical functions tabulated in [34], as a function of the spin parameter and species of Hawking particle (photons, neutrinos, gravitons). Setting $a_* = 1$ and $M = 10^8\ M_\odot$, we find the spindown rate to be $\dot{a}_* \approx -7 \times 10^{-97}\mathrm{s}^{-1}$. At that rate, the spin will remain high enough to allow Planck-scale BSW reactions for a Hubble time. However, the strong mass scaling means that, for stellar-mass black holes of $M \sim 10\ M_\odot$, the spindown rate would be on the order of $\dot{a}_* \approx 10^{-75}\mathrm{s}^{-1}$. While this still sounds extremely small (i.e., the spin will remain near-extremal for a very long time), let us review the c.o.m. scaling with spin.

For spin $a_* = 1 - \epsilon$, the critical angular momentum (maximum c.o.m. energy) for incoming particles is $b_{\mathrm{crit}} \approx 2(1 + \epsilon^{1/2})$. The critical radius for these collisions is at $r_{\mathrm{crit}} \approx 1 + 2\epsilon^{1/2}$, and the c.o.m. energy scales like $E_{\mathrm{COM}} \approx (r-1)^{-1/2} \approx \epsilon^{-1/4}$ [19, 21]. So for an incoming particle with rest mass on the order of a GeV, in order to reach Planck energies ($\sim 10^{19}$ GeV) the critical spin is $1 - a_* \lesssim 10^{-76}$. In other words, an extremal stellar-mass black hole would spin down from Hawking radiation in under a second (however, see below in Sec. 3 for a less conservative limit on the critical spin value).

Focusing for now on the supermassive black holes, where Hawking radiation should not be important, there is however another, more astrophysical mechanism to spin down the black hole. All astrophysical black holes are surrounded by a bath of isotropic thermal radiation from the cosmic microwave background. At a present temperature of 2.73 K, this radiation is far more energetic than the Hawking radiation from any black hole larger than the mass of the moon ($\sim 10^{-8} M_\odot$). Furthermore, it is isotropic, so a Kerr black hole will preferentially absorb photons with negative angular momentum, thereby accelerating the spin-down process.

From numerical calculations with the Pandurata ray-tracing code [35], we can determine the cross-section of an extremal black hole to radiation incoming from infinity, and find an angle-averaged effective radius of $r_{\mathrm{eff}} \approx \sqrt{23} r_g$, with the gravitational radius of a black hole defined by $r_g = GM/c^2$. We found the mean specific angular momentum of a captured photon to be $-1.6 r_g$. So following from equation (16) we get

$$\frac{da_*}{dt} = -2a_*\frac{\dot{M}}{M} + \frac{\dot{J}}{M^2} = -3.6\frac{\dot{M}}{M} = 4 \times 10^{-36}\left(\frac{T}{2.73\ \mathrm{K}}\right)^4\left(\frac{M}{10^8\ M_\odot}\right)\mathrm{s}^{-1}, \tag{17}$$

where the final expression comes from the "accretion" of the CMB flux $\dot{M}c^2 = 4\pi r_{\rm eff}^2 \sigma T^4$. A smaller but similar level of flux is received from the cosmic neutrino background.

Clearly, the effect of CMB accretion dominates over Hawking radiation for any astrophysical black hole. Even for the smallest known black holes, an initially extremal black hole would spin down well below the critical BSW/Planck spin value in a tiny fraction of a second.

In addition to these many critiques and commentaries on BSW, there has been an even larger number of follow-on papers exploring analogous effects in non-Kerr black holes. These papers were both within the limits of general relativity (e.g., Kerr-Newman metric), as well as alternative theories of gravity. However, since this review (and the entire Topical Collection) is specifically concerned with the Kerr metric, we consider these alternative approaches to be outside the scope of our present discussion.

3 Super-Penrose Process

One of the most interesting aspects of the post-BSW literature is the question of the range of energies and escape fraction of the reaction products. As discussed above, the original limit of Wald [6] was only 121% for the spontaneous decay of a massive particle into two photons. To better understand the range of attainable energies and their relative likelihoods, we introduce a novel graphical representation of the reaction products. In the interest of tractability of a many-dimensional problem, for this entire section, unless otherwise stated, we will restrict our analysis to planar equatorial trajectories for extremal Kerr black holes.

In Figure 5 we show an example of this graphic for the classical Penrose process of a single particle decay. Following our approach in [36], each image corresponds to a specific choice of initial mass, energy, angular momentum, and distance from the black hole. The polar coordinates are defined in the particle's frame (or center-of-mass frame for collisional reactions), with the coordinate radial direction oriented to the right. The color represents the energy-at-infinity of the daughter photons as a function of emission angle, and the radius of the disk represents whether or not that photon escapes ($R = 1$), is captured by the black hole horizon ($R = 0.8$), or has negative energy ($R = 0.6$), in which case it will be also be captured by the black hole.

First of all, note that we are following the convention of Section 2, where we consider reactions of the form

$$\mathbf{p}^{(1)} + \mathbf{p}^{(2)} \rightarrow \mathbf{p}^{(3)} + \mathbf{p}^{(4)}. \tag{18}$$

Particles 1 and 2 collide and produce particles 3 and 4. In the center of mass frame, where all these polar plots are calculated, particles 3 and 4 are always emitted in opposite directions. For the classical Penrose decay process, we can still use the formalism of equation (18), with particles 1 and 2 having identical trajectories and each one has exactly half of the total initial energy. In the first frame of Figure 5, the decay takes place at $r = 10M$, relatively far from the black hole. The incoming particle is falling from rest at infinity, and has the critical value

of angular momentum $b_1 = 2$. Thus the photons emitted in the forward-pointing, $-\hat{r}$ direction have slightly higher energy due to Doppler boosting. We can also see that roughly 20% of all emitted photons are captured by the black hole, preferentially those with negative angular momentum.

The middle frame of Figure 5 corresponds to a decay at $r = 1.9999M$, just inside the ergosphere. At this point, we see the first genuine Penrose process reaction, with the forward-going particle having an energy just over unity, and the opposite particle has a very slightly negative energy (the tiny notch in the polar plot at $\phi \approx 315°$). In the third frame, the reaction takes place deep in the ergosphere, and the Wald limit is reached with forward-pointing particles escaping with energy of $E_3 = 1.21E_1$. It is interesting to note that, even this close to the event horizon, when the initial particle has the critical value for angular momentum, a majority (≈ 53%) of the decay products are still able to escape the black hole.

Next we turn to the collisional cases, starting with the analysis of Bejger *et al.* [22]. As mentioned briefly above, they focus on the energy of the particles that can eventually escape to infinity. They also restrict their considerations to identical, massive particles falling from rest at infinity ($E_1 = E_2 = 1$) and particle one has a critical value of angular momentum $b_1 = 2$. Both daughter particles are massless, so we also refer to the process as annihilation. In Figure 6 we show the peak energy for E_3 as a function of reaction radius for a range of select values of b_2. The peak quickly asymptotes to ~ 130%, only marginally higher than that of a single particle decay. Ref. [37] derives this efficiency analytically as $\eta = (1 + \sqrt{3} + \sqrt{6})/4$.

In Figure 7 we show similar results, but with our polar energy plots for a range of annihilation radii, while keeping the initial particle properties fixed: $b_1 = 2$ and $b_2 = -2$. In all cases, both particles are on inward-moving trajectories $p_r < 0$, denoted in the figure with a '−' sign for the parameter σ_{r1}. While the c.o.m. energy grows with decreasing radius, the escape fraction is significantly reduced, and most of the high-energy particles are captured by the black hole. As described in [22], even the escaping particles are actually initially emitted with $p_r < 0$, but reflect off of the centrifugal barrier of the black hole before escaping to infinity. This is not entirely obvious in Figure 7, which shows the angular distribution as measured in the particle's center-of-mass frame. Deep into the particles' plunge, even the particles emitted in the $+r$ direction of the polar plots in fact have inward-moving trajectories in the coordinate frame.

Completely independent, and largely ignorant, of the flurry of papers surrounding BSW, at that time we were working on calculating the phase space distribution and annihilation rates of dark matter particles around a spinning black hole [38]. Adhering to the well-known strategy of "if your only tool is a hammer, everything looks like a nail," we developed a version of the Pandurata ray-tracing code [35] to calculate fully 3-dimensional trajectories of massive test particles coming in from rest at infinity. A sample of these particles will annihilate, and then we follow the photon trajectories either to the horizon or escape to infinity.

Curiously, some of these escaping photons would have very large energy, ten times greater than the rest mass of the dark matter particles, in clear contradiction to the analytic

predictions of [22, 23]. After months of searching for bugs and mathematical errors, we were forced to accept the results as physically real, and were then able to isolate and identify the cause of the discrepancy with the analytic results. The difference was really quite simple: all previous studies had limited their attention to incoming particles with critical values for $b_1 = 2$, allowing the particles to get as close as possible to the event horizon in order to maximize the center-of-mass energy. Yet the numerical approach naturally included a much greater sample of phase space, including particles with $b_1 > 2$ that reflected off the centrifugal barrier before colliding with other incoming particles. It was these outgoing, super-critical particles responsible for the escaping high-energy annihilation products, and thus we call them *super-Penrose* processes.

As with the ingoing trajectories, the c.o.m. energy of the outgoing particles also is maximized near the horizon, so we want to focus on near-critical particles with $b_1 \approx 2$. We can now return to an analytic approach, simply changing the sign for the radial momentum in equation (11). The results are plotted in Figure 8, showing the peak efficiency as a function of radius for a selection of b_2 values. Recall our definition of efficiency is "total energy out divided by total energy in," so a photon that escapes with $\eta = 6.37$ actually has an energy of $\approx 13 \times m_1$, in agreement with the results found accidentally in [38]. As with the ingoing annihilation, an analytic expression was derived in [37]: $\eta_{\max} = (2 + \sqrt{3})(2 + \sqrt{2})/2$.

The difference between $p_r^{(1)} > 0$ and $p_r^{(1)} < 0$ is also shown in the polar plots of Figure 9, corresponding to the blue curve in Figure 6 and the dark red curve of Figure 8. All parameters are identical, except one has an outgoing particle 1. This small detail makes a very big difference in the center of mass energy [$1.89(E_1 + E_2)$ vs $4.49(E_1 + E_2)$], escape fraction (20% vs 35%), and peak efficiency (122% vs 278%). Note that the other parameters, in particular b_2 and r, are not specifically chosen to optimize energy efficiency, but rather as a representative sample of the literature.

In Figure 10 we show the energy and escape distributions for collisions tuned to maximize efficiency. The choice of $b_2 = -2$ leads to more head-on collisions, and nicely demonstrates the nearly symmetric distribution of annihilation product energies due to the zero net angular momentum of the initial particles [$b_2 = -2(1 + \sqrt{2})$ gives an even greater energy, but is less symmetric and has a slightly smaller escape fraction].

We showed in [11] that the absolute maximum efficiency is achieved for Compton-like scattering between an outgoing photon with $b_1 = 2$ and an infalling massive particle with $b_2 = -2(1 + \sqrt{2})$. The post-scatter products are an in-going photon with $b_3 = 2$ and an in-going massive particle with negative energy and angular momentum. Figure 11 shows the energy and escape distributions for these Compton scattering reactions, for a range of photon energy E_1. In the limit of $E_1 >> E_2$ and $r \rightarrow r_+$, the absolute maximum efficiency for Compton scattering is given by $\eta = (2 + \sqrt{3})^2 \approx 1392\%$ [37]!

The most remarkable feature of this particular configuration is that, after the scattering event, the photon—now boosted by in energy by a factor of $\gtrsim 10$— is on an in-going trajectory, reflects off the black hole's centrifugal barrier, and then becomes an out-going

photon. At this point, it can scatter off a new infalling massive particle. In this way, the panels of Figure 11 can be considered as three consecutive scattering events, each photon getting boosted to a higher energy, while the massive particles all have the same basic energy.

By including these multiple scattering events, the net efficiency can grow without limit. Well, almost without limit. We also showed in [11] that each step in this scattering process deposits more negative energy and angular momentum into the black hole, resulting in its eventual spin-down. Recall from Section 2 above, for an incremental decrease in spin ϵ, the critical impact parameter for reflection increases to $b_{\rm crit} \approx 2(1 + \epsilon^{1/2})$, steadily pushing the location for high-efficiency collisions farther from the horizon. Taking each scattering event as an increase in photon energy of a factor of 10, the spin parameter after N scatters is given by [11]

$$1 - a_* = \epsilon_{N+1} \approx (4 + 2\sqrt{2})N\frac{m_2}{M}\,. \tag{19}$$

The requirement that the scattering event occurs outside of $r_{\rm crit}$ leads to a condition on the maximum number of such events to be $N_{\rm max} \approx \log_{10}(M/m_2)^{1/2}$ (note also in Figure 11 how each higher energy requires collision at a smaller radius in order to achieve the target 10× increase in energy). Taking m_2 to be the electron mass and $M = 10M_\odot$ gives $N_{\rm max} \approx 30$, for a peak energy of 10^{26} GeV. Thus photons undergoing repeated Compton scattering events could not only far surpass the Planck energy scale, but these hyper-energetic photons could even escape to an observer at infinity! Furthermore, by accelerating the photons to high energy one step at a time, it avoids the BSW limit derived above of $\epsilon \lesssim 10^{-76}$ to a much larger $\epsilon \lesssim 10^{-59}$. Unfortunately, this is still too small for an astrophysical black hole to attain due to the rapid accretion of CMB photons and neutrinos, but perhaps might still be attainable in a properly shielded laboratory environment.

Following shortly after the discovery of these super-Penrose reactions, Berti *et al.* [39] found solutions with even greater efficiencies (aptly named “super-Schnittman” reactions), but only for trajectories that were not obtainable with particles falling in from infinity. Specifically, they consider very similar configurations to the Compton scattering described above, with $p_r^{(1)} > 0$ and $p_r^{(2)} < 0$, but now with $b_1 < 2$, which is only possible if particle 1 originates in the ergosphere via some other scattering process [39, 40]. The greatest efficiency is found for the greatest deviation from the critical value of $b_{\rm crit} = 2$. Unfortunately, the larger the deviation, the harder it is to produce such a particle by colliding “normal” particles falling in from infinity.

We reproduce some of the results of [39] in Figure 12 for hypothetical massive particles with $b_1 = b_2 = 0$ annihilating in the ergosphere, with particle 1 on an out-going trajectory. With this selection of *deus ex machina* particles, it is easy to reach very high values for $E_{\rm com}$, $\eta_{\rm max}$, and also the escape fraction. While it is impossible for these out-going trajectories to originate from initially infalling particles, [39] proposes an alternative source: the products of earlier scattering reactions. However, for the simple cases they explore, the infalling rest

mass must be sufficiently large to produce the appropriate out-going trajectories, so that in the end, the net efficiency is no greater than the single rebound configuration we originally proposed in [11]

Before we move on to the next section, covering more generic numerical calculations of the Penrose process, it is valuable to discuss in more detail the analytic results of Leiderschneider & Piran [37]. Unlike the vast majority of papers cited thus far, [37] extends their analysis to also include non-planar trajectories. The reactions still take place in the equatorial plane, but the reactant particles themselves are allowed to move out of the plane (for the case of reactions outside of the plane, see [41]). In doing so, they were able to dispell one of the popular assumptions made in many previous works: due to symmetry, the highest energies must come from purely planar trajectories. For example, the "standard" BSW case of massive, infalling planar particles annihilating into photons just outside the horizon gives a peak efficiency of 130% [22]. By relaxing only the condition on the location of the collision, slightly larger values of b_1 are allowed, and the resulting efficiency increases significantly: $\eta_{\max} \approx 2.63$ [37] (see also [42] who correctly identify the important problem of taking the r, b limits in the proper order, but appear to make an arithmetic error and obtain a slightly smaller efficiency). This actually makes perfect sense: by selecting the largest possible value for b_1 for a given radius, we are in effect setting the radial velocity to zero, because that radius corresponds to a turning point for that impact parameter. Therefore the efficiency naturally lies somewhere between the ingoing and outgoing results.

Relaxing the initial conditions further, so that the incoming particles have some motion in the θ-direction, gives a larger available center-of-mass energy, again increasing the efficiency. However, it appears that this approach only works for ingoing particles with $b_1 = 2$ and $p_r^{(1)} < 0$ (these non-planar orbits with critical values of b were also identified in [43]). For $p_r^{(1)} > 0$, the maximum energy and efficiency are still realized with fully planar trajectories [37].

In Table 1 we reproduce a summary of the analytic results for peak efficiency from Ref. [37], combining their Tables 1 and 2. We follow their notation describing the parameters of collisions as massive particles 'M' and 'm', photons 'P' and 'p', and the direction of particle 1 (positive or negative radial velocity). When particle 2 has mass 'm', this means that one should take the limit of $E_1 >> m$. Similarly, when particle 2 is a photon of energy 'p', this corresponds to $M_1 >> p$ (these results for "heavy" massive particles were derived independently by [44]). For massive products, we also list the peak rest mass attainable for particle 3, which does not necessarily correspond to the same trajectories used to achieve peak efficiency [37].

As can be seen from the results in Table 1, the absolute maximum efficiency is still that discovered in [11]. But we also see that generally, high-efficiency collisions can be realized for a wide variety of generic reactions. The unifying theme appears to be the critical angular momentum for particle 1, along with near-horizon collisions around extremal black holes.

4 Numerical Calculations

Compared to the extensive analytic work described in the previous section, there have been significantly fewer numerical studies of the Penrose process. Yet for just about any astrophysical application, full 3D (6D in phase space) calculations are required to predict observable features of the reaction products. Astrophysical applications will also require the use of generic spin parameters, as opposed to the maximal spin limit.

The first such attempt at a numerical calculation was done in the seminal paper by Piran and Shaham [7], where they did a Monte Carlo simulation of the particles produced by elastic scattering of infalling protons with identical particles on stable circular planar orbits. While extremely impressive for the time, computational limitations restricted their calculations to a few thousand protons, enough to get a qualitative feel for the spectral properties and Penrose process rates, but hardly enough to fully sample the phase space. One representative example is shown in Figure 13. This shows the outgoing energy spectrum for particle 3, also massive in this example. The black hole spin is $a_* = 0.998$, particle 2 is on a bound circular orbit at the ISCO, and particle 1 falls in from infinity with zero angular momentum. Of the 2000 protons participating in the 1000 collisions included in their calculation, only 23 escape with energy greater than $E_1 + E_2 = 1.674 M_p c^2$.

Nearly 20 years later, with significant advances in computing power, a more comprehensive study was carried out in [45], covering a wider range of collisional cases, including pair production, Compton scattering, and gamma-ray-proton pair production ($\gamma + p \rightarrow p + e^- + e^+$). Again, the focus was on astrophysical applications, so the canonical spin of $a_* = 0.998$ was used. This work was further expanded in [46], exploring the range of angles and energy for outgoing photons.

While these earlier works were able to explore a much wider range of parameter space for the collision products, they were still generally limited to a relatively small number of specific *initial* conditions for the reactants. In [38] this author attempted to expand on this approach and carry out a numerical calculation of the full 6D distribution of both reactants and products for annihilation events around spinning black holes. Using the radiation transport code Pandurata to integrate geodesic trajectories, we populate the phase space by launching a large number of test particles around the black hole. At each time step along the trajectory, a weighted contribution is added to the 6-dimensional phase space (in practice, "only" 5-dimensional, because of the azimuthal spatial symmetry of the Kerr metric).

We divide the distribution into two populations: bound and unbound. The unbound population has a thermal, non-relativistic velocity distribution at infinity. The bound population is constructed to produce a power-law slope in density, and only includes particles on stable orbits with specific energy less than unity, isotropic as seen local quasi-stationary observer, with a Maxwell-Juttner velocity distribution and characteristic energy corresponding to a virial temperature. In principal, any slope can be produced, but we generally restrict ourselves to $\rho \sim r^{-2}$ following [47, 48].

The main results of this calculation are shown in Figure 14, reproduced from [38]. The contour plots show 2D cuts in the (r, θ) plane of the density distribution for bound and

unbound populations, for spin parameters of $a_* = 0$ and $a_* = 1$. Because of the numerical nature of this approach, any spin can be used, but these obviously span the range of astronomical possibilities. The density distribution of the bound population agrees closely with the analytic results of [48] for nonspinning black holes, and [49] for the Kerr case. It is interesting to note that for the spinning case, the unbound density distribution is almost perfectly uniform in θ, rising steadily towards the horizon, despite the fact that many of these particles spend a large amount of coordinate time orbiting near the midplane before finally plunging. On the other hand, the bound population shows a clear break in symmetry, due to the increased stability of prograde, planar orbits. These orbits contribute to a density spike in the form of a thick torus, peaking around radius $r = 4M$ [38].

In addition to the density distribution $\rho(r, \theta)$, we also calculate the distribution in velocity space at each point. These results are shown in Figures 15 and 16 for the unbound and bound populations, respectively. In all cases, the velocities are measured by an observer in the equatorial plane at radius $2M$. For the unbound population, the observer is free-falling from infinity (FFIO) with zero angular momentum; for the bound population, the observer has no radial motion, but rotates with the spin of the black hole despite zero angular momentum (LNRF, locally non-rotating frame in the language of [5]).

Despite the fact that the spatial density distribution for unbound particles appears quite uniform in θ in Figure 14, we see that the velocity distribution near the black hole is not at all isotropic. There is essentially a bimodal distribution of velocity, with retrograde particles plunging with large negative values of v^r, and prograde particles corating with the black hole spin, peaked around $v^r = 0$ and $\gamma v^\phi = c$.

As can be seen in Figure 16, the bound population is much more isotropic. This is hardly surprising, as there are no stable retrograde orbits at $r = 2M$, and even the prograde orbits are almost perfectly planar and circular, spanning a narrow range of velocity as seen by a nearly stationary, LNRF observer.

5 Dark Matter Applications

Despite the wide variety of fundamental and fascinating results described in the previous sections, by most accounts the collisional Penrose process is unlikely to play a significant role in astrophysical processes. Even the highest efficiency reactions can only provide energy boosts on the order of a factor of ten or so, far below the ultrarelativistic particles seen from gamma-ray bursts or active galactic nuclei[1]. And in any case, even those moderately high-efficiency events require such fine tuning of initial conditions, they are probably impossible to realize in a natural setting.

One potential (although admittedly speculative) exception is the annihilation of dark matter (DM) particles in the ergosphere around a Kerr black hole. Numerous authors have pointed out the important role that supermassive black holes might play in shaping the DM density profile around galactic nuclei [47,51–54]. However, in almost all these cases, the enhanced

[1]A leading theory for magnetically powered jets is the Blandford-Znajek process [50], which does extract energy from the spin of the black hole, but not through a particle-based Penrose process.

DM density—and thus annihilation signal—is a purely Newtonian effect, and is therefore not within the scope of this review.

However, if the DM density profile is sufficiently steep, or the annihilation cross section increases with energy (e.g., through p-wave annihilation [55]), then the annihilation signal will be dominated by reactions closest to the black hole, where relativistic effects *are* important. With the full phase-space distribution function calculated as in the previous section, in [38] we were able to calculate the outgoing spectrum from a sample of possible annihilation models. One simple model is where the cross section for annihilation increases greatly above a certain threshold energy, analogous to pion creation via proton-proton reactions. With the Monte Carlo code Pandurata, we can sample the phase space of test particles from both bound and unbound populations, and calculate annihilation rates for a given cross section model. The simplest annihilation model produces two photons of equal energy and isotropic in angle in the center-of-mass frame of the reacting DM particles. These photons are then propogated to an observer at infinity, where they can be summed to produce images and spectra.

If we take the threshold center-of-mass energy to be a moderate $3m_\chi c^2$, we find that most of the annihilation photons are produced within the ergosphere region, and are thus sensitive probes of the Penrose process. In Figure 17 we show a simulated image produced by the annihilation photons produced from the unbound DM population around an extremal Kerr black hole, as seen by an observer at infinity and inclination of 90° from the spin axis. The extreme frame dragging and Doppler boosting from prograde orbits make the image highly asymmetric. Clearly visible is the characteristic shadow of a Kerr black hole, with a flattened prograde edge, as described in [12].

In Figure 18 we show the spectra corresponding to this annihilation scenario, for a range of black hole spins, for both the unbound and bound populations. In order to highlight the effects of the black hole spin, we focus on reactions coming from close to the black hole. For the unbound population, this means using an energy threshold for the annihilation cross section of $E_{\rm com} > 3m_\chi c^2$. For the bound population, no threshold is needed, as the density peak near the black hole naturally leads to the annihilation signal being dominated by photons coming from small r. Note the qualitatively different spin dependences in the two cases: for unbound DM particles, the low energy part of the spectrum is independent of spin, as all these photons come from plunging particles near the horizon, and experience significant gravitational redshift. At the high energy end, we see the clear importance of spin in generating high-efficiency, extreme Penrose process reactions. For the bound population, on the other hand, the stable orbits do not intersect with very large c.o.m. energies, so even for very high spins we do not see much influence from the Penrose process. Yet the spin does play an important role in shaping the low-energy end of the spectrum, as higher spins allow stable orbits closer to the horizon, and thus more extreme gravitational redshift, just as in the case of the red tail of the iron flourescent lines seen around black holes of all sizes [56].

The overall vertical axes in Figure 18 are arbitrary, because we still don’t know very much about the overall density scaling of DM distributions around black holes. Even more

uncertain is the amplitude of the annihilation cross section, much less its energy dependence. We hope that in the future, as gamma-ray telescopes improve in angular and energy resolution, we will be able to use quiescent black holes in galactic nuclei to probe the properties of the DM particle, measure black hole spins, and explore the exotic physics that describe the ergosphere. Perhaps one day we might even discover advanced civilizations that have successfully harnessed the black hole spin as an energy source, as imagined by Penrose in his original paper [3]!

6 Discussion

We have provided a broad overview of some of the recent work on the collisional Penrose process, with particular focus on collisions around extremal Kerr black holes. Despite the numerous astrophysical limitations, since the publication of BSW [13], there has been a great deal of interest in determining the highest attainable collision efficiencies. These high-efficiency reactions require both large center-of-mass energies and also fine tuning of the reaction product trajectories in order to assure they can escape from the black hole. While non-Kerr (or even non-GR) black holes could more generally lead to diverging center-of-mass energies, we have restricted this review to classical, if extremal, Kerr black holes.

For more general astrophysical observations, dark matter annihilation appears to be one of the more promising applications of the Penrose process. One reason for this is that DM particles are most likely to travel along perfect geodesics, even in the presence of the diffuse gas and strong magnetic fields typically found around astrophysical black holes. Additionally, the DM density distribution is expected to peak near galactic nuclei, which also contain supermassive black holes. Lastly, the extreme gravitational field of the black hole is a promising mechanism to enhance annihilation, both through increasing the relative collision energy, and also through gravitational focusing that increases the DM density.

As with the question of peak efficiency for Penrose collisions, an important factor in the observability of DM annihilation around black holes is the question of the escape fraction for the resulting reaction products. We showed above in Section 3 the planar escape distribution for a selection of specially chosen collisions. More general calculations of the escape probability have been carried out in [57–59]. In short, the escape fraction decreases as the distance from the black hole decreases (and thus the center-of-mass energy increases). This is true for particles plunging in from infinity. But for particles on stable, bound orbits, the escape fraction can actually be quite large, on the order of 90% or more [38, 36].

In most previous work on the subject, and in our own discussion above, the DM population is generally divided into bound, and unbound. However, when including self-interactions (e.g., [60]), these two populations can mix, giving rise to new phenomenology and potentially greater enhancements of the annihilation signal [52–54]. Exotic DM particle models with energy-dependent annihilation cross sections (e.g., [55,61,62]) promise to make this field one of active research in the years to come.

Aside from DM annihilation, astrophysical applications of the classical, collisional Penrose process are limited. In particular, from everything we have seen in the review, extremely fine

tuning and multiple collisions would be required to get anywhere close to the high-energy gamma-rays (or even cosmic rays) seen from many active galactic nuclei. On the other hand, the high-energy emission that is observed is likely indirectly related to the Penrose process, by general coupling matter to the spin of the black hole. This can be done far more efficiently when employing large-scale fields, either in the form of super-radiance [63,64], or coupling the particles directly to electromagnetic fields that in turn penetrate the black hole horizon [50,65]. Unfortunately, the high efficiency of these mechanisms at creating gamma-rays only serves to confuse and complicate any prospects of direct detection of DM annihilation around otherwise quiescent galactic nuclei. We look forward to the next generation of high-energy observatories that will be able to circumvent these confusion sources with greater sensitivity, and improved spatial and energy resolution.

Acknowledgements

We thank Alessandra Buonanno, Francese Ferrer, Ted Jacobson, Henric Krawczynski, Tzvi Piran, Laleh Sadeghian, and Joe Silk for helpful comments and discussion. A special thanks to the editor of this Topical Collection, Emanuele Berti, for his encouragement and patience.

References

1. Kerr RP, Physical Review Letters 11, 237 (1963). DOI 10.1103/PhysRevLett.11.237
2. Boyer RH, Lindquist RW, Journal of Mathematical Physics 8, 265 (1967). DOI 10.1063/1.1705193
3. Penrose R, Nuovo Cimento Rivista Serie 1 (1969)
4. Christodoulou D, Physical Review Letters 25, 1596 (1970). DOI 10.1103/PhysRevLett.25.1596
5. Bardeen JM, Press WH, Teukolsky SA, Astrophysical Journal 178, 347 (1972). DOI 10.1086/151796
6. Wald RM, Astrophysical Journal 191, 231 (1974). DOI 10.1086/152959
7. Piran T, Shaham J, Phys. Rev. D16, 1615 (1977). DOI 10.1103/PhysRevD.16.1615
8. Novikov ID, Thorne KS, in Black Holes (Les Astres Occlus), ed. by Dewitt C, Dewitt BS (1973), pp. 343–450
9. Thorne KS, ApJ 191, 507 (1974). DOI 10.1086/152991
10. Piran T, Shaham J, Katz J, Astrophys. J. Lett196, L107 (1975). DOI 10.1086/181755
11. Schnittman JD, Physical Review Letters 113(26), 261102 (2014). DOI 10.1103/PhysRevLett. 113.261102. 1410.6446 [PubMed: 25615298]
12. Chandrasekhar S, The mathematical theory of black holes (1992)
13. Bañados M, Silk J, West SM, Physical Review Letters 103(11), 111102 (2009). DOI 10.1103/ PhysRevLett.103.111102. 0909.0169 [PubMed: 19792361]
14. Visser M, ArXiv e-prints (2007). 0706.0622
15. Lake K, Physical Review Letters 104(21), 211102 (2010). DOI 10.1103/PhysRevLett.104.211102. 1001.5463 [PubMed: 20867083]
16. Gao S, Zhong C, Phys. Rev. D84(4), 044006 (2011). DOI 10.1103/PhysRevD.84.044006. 1106.2852
17. Stuchlík Z, Schee J, Classical and Quantum Gravity 30(7), 075012 (2013). DOI 10.1088/0264-9381/30/7/075012
18. Harada T, Kimura M, Classical and Quantum Gravity 31(24), 243001 (2014). DOI 10.1088/0264-9381/31/24/243001. 1409.7502
19. Berti E, Cardoso V, Gualtieri L, Pretorius F, Sperhake U, Physical Review Letters 103(23), 239001 (2009). DOI 10.1103/PhysRevLett.103.239001. 0911.2243 [PubMed: 20366184]
20. Harada T, Kimura M, Phys. Rev. D83(2), 024002 (2011). DOI 10.1103/PhysRevD.83.024002. 1010.0962

21. Jacobson T, Sotiriou TP, Physical Review Letters 104(2), 021101 (2010). DOI 10.1103/PhysRevLett.104.021101. 0911.3363 [PubMed: 20366583]
22. Bejger M, Piran T, Abramowicz M, Håkanson F, Physical Review Letters 109(12), 121101 (2012). DOI 10.1103/PhysRevLett.109.121101. 1205.4350 [PubMed: 23005933]
23. Harada T, Nemoto H, Miyamoto U, Phys. Rev. D86(2), 024027 (2012). DOI 10.1103/PhysRevD.86.024027. 1205.7088
24. Ding C, Liu C, Quo Q, International Journal of Modern Physics D 22, 1350013 (2013). DOI 10.1142/S0218271813500132. 1301.1724
25. Galajinsky A, Phys. Rev. D88(2), 027505 (2013). DOI 10.1103/PhysRevD.88.027505
26. Zaslavskii OB, Phys. Rev. D88(10), 104016 (2013). DOI 10.1103/PhysRevD.88.104016. 1301.2801
27. Patil M, Joshi PS, Nakao K.i., Kimura M, Harada T, EPL (Europhysics Letters) 110, 30004 (2015). DOI 10.1209/0295-5075/110/30004. 1503.08331
28. Grib AA, Pavlov YV, Gravitation and Cosmology 17, 42 (2011). DOI 10.1134/S0202289311010099. 1010.2052
29. Mc Caughey E, European Physical Journal C 76, 179 (2016). DOI 10.1140/epjc/s10052-016-4028-6. 1603.08774
30. Hod S, Physics Letters B 759, 593 (2016). DOI 10.1016/j.physletb.2016.06.028. 1609.06717
31. Thorne KS, Magic without magic. J.-A.-Wheeler: A collection of essays in honor of his sixtieth birthday. (1972)
32. Bekenstein JD, Phys. Rev. D7, 2333 (1973). DOI 10.1103/PhysRevD.7.2333
33. Hawking SW, Communications in Mathematical Physics 43, 199 (1975). DOI 10.1007/BF02345020
34. Page DN, Phys. Rev. D14, 3260 (1976). DOI 10.1103/PhysRevD.14.3260
35. Schnittman JD, Krolik JH, Astrophys. J.777, 11 (2013). DOI 10.1088/0004-637X/777/1/11. 1302.3214
36. Schnittman JD, Silk J, Phys. Rev. D(2018)
37. Leiderschneider E, Piran T, Phys. Rev. D93(4), 043015 (2016). DOI 10.1103/PhysRevD.93.043015. 1510.06764
38. Schnittman JD, Astrophys. J.806, 264 (2015). DOI 10.1088/0004-637X/806/2/264. 1506.06728
39. Berti E, Brito R, Cardoso V, Physical Review Letters 114(25), 251103 (2015). DOI 10.1103/PhysRevLett.114.251103. 1410.8534 [PubMed: 26197116]
40. Zaslavskii OB, Phys. Rev. D93(2), 024056 (2016). DOI 10.1103/PhysRevD.93.024056. 1511.07501
41. Gariel J, Santos NO, Silk J, Phys. Rev. D90(6), 063505 (2014). DOI 10.1103/PhysRevD.90.063505. 1409.3381
42. Harada T, Ogasawara K, Miyamoto U, Phys. Rev. D94(2), 024038 (2016). DOI 10.1103/PhysRevD.94.024038. 1606.08107
43. Harada T, Kimura M, Phys. Rev. D83(8), 084041 (2011). DOI 10.1103/PhysRevD.83.084041. 1102.3316
44. Zaslavskii OB, Phys. Rev. D94(6), 064048 (2016). DOI 10.1103/PhysRevD.94.064048. 1607.00651
45. Williams RK, Phys. Rev. D51, 5387 (1995). DOI 10.1103/PhysRevD.51.5387
46. Williams RK, ArXiv Astrophysics e-prints (2002). astro-ph/0203421
47. Gondolo P, Silk J, Physical Review Letters 83, 1719 (1999). DOI 10.1103/PhysRevLett.83.1719. astro-ph/9906391
48. Sadeghian L, Ferrer F, Will CM, Phys. Rev. D88(6), 063522 (2013). DOI 10.1103/PhysRevD.88.063522. 1305.2619
49. Ferrer F, Medeiros da Rosa A, Will CM, Phys. Rev. D96(8), 083014 (2017). DOI 10.1103/PhysRevD.96.083014. 1707.06302
50. Blandford RD, Znajek RL, Mon. Not. Royal Astron. Soc179, 433 (1977). DOI 10.1093/mnras/179.3.433

51. Merritt D, Milosavljevic M, Verde L, Jimenez R, Physical Review Letters 88(19), 191301 (2002). DOI 10.1103/PhysRevLett.88.191301. astro-ph/0201376 [PubMed: 12005623]
52. Fields BD, Shapiro SL, Shelton J, Physical Review Letters 113(15), 151302 (2014). DOI 10.1103/PhysRevLett.113.151302. 1406.4856 [PubMed: 25375700]
53. Shapiro SL, Paschalidis V, Phys. Rev. D89(2), 023506 (2014). DOI 10.1103/PhysRevD.89.023506. 1402.0005
54. Shapiro SL, Shelton J, Phys. Rev. D93(12), 123510 (2016). DOI 10.1103/PhysRevD.93.123510. 1606.01248 [PubMed: 29881789]
55. Feng JL, Kaplinghat M, Yu HB, Phys. Rev. D82(8), 083525 (2010). DOI 10.1103/PhysRevD.82.083525. 1005.4678
56. Reynolds CS, Nowak MA, Physics Reports 377, 389 (2003). DOI 10.1016/S0370-1573(02)00584-7. astro-ph/0212065
57. Williams AJ, Phys. Rev. D83(12), 123004 (2011). DOI 10.1103/PhysRevD.83.123004. 1101.4819
58. Bañados M, Hassanain B, Silk J, West SM, Phys. Rev. D83(2), 023004 (2011). DOI 10.1103/PhysRevD.83.023004. 1010.2724
59. Ogasawara K, Harada T, Miyamoto U, Igata T, Phys. Rev. D95(12), 124019 (2017). DOI 10.1103/PhysRevD.95.124019. 1609.03022
60. Spergel DN, Steinhardt PJ, Physical Review Letters 84, 3760 (2000). DOI 10.1103/PhysRevLett.84.3760. astro-ph/9909386 [PubMed: 11019199]
61. Chen J, Zhou YF, Cosmology J and Astro. Phys 4, 017 (2013). DOI 10.1088/1475-7516/2013/04/017. 1301.5778
62. Zurek KM, Phys. Reports 537, 91 (2014). DOI 10.1016/j.physrep.2013.12.001. 1308.0338
63. Press WH, Teukolsky SA, Nature 238, 211 (1972). DOI 10.1038/238211a0
64. Brito R, Cardoso V, Pani P (eds.). Superradiance, Lecture Notes in Physics, Berlin Springer Verlag, vol. 906 (2015)
65. Wagh SM, Dhurandhar SV, Dadhich N, Astrophys. J.290, 12 (1985). DOI 10.1086/162952

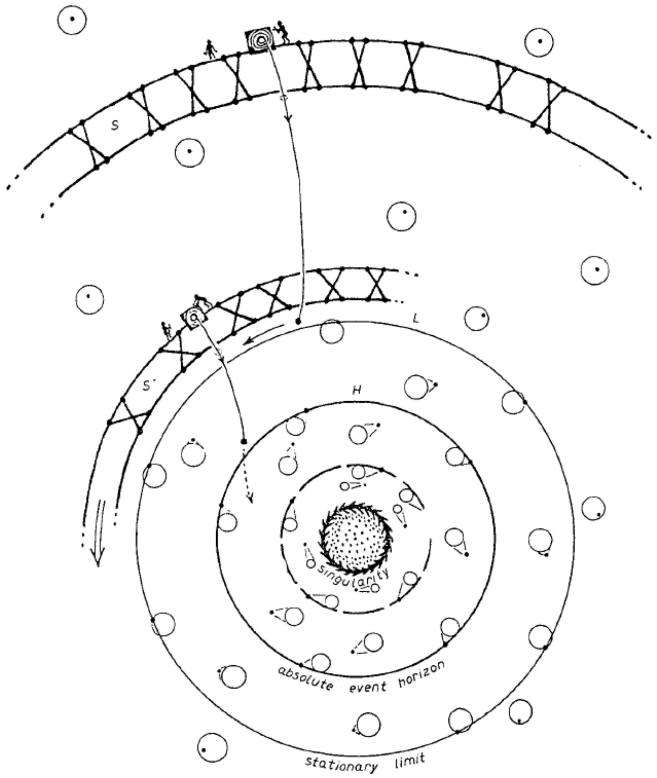

Fig. 1.

Potential application of the Penrose process for energy extraction from a spinning black hole with macroscopic particles. The image depicts concentric rings of superstructures orbiting the black hole, with people lowering masses on pulleys to extract gravitational energy from the mass. Inside the ergosphere (marked “static limit” in this figure), these packages can attain negative energy, and thus greater than unity efficiency in energy generation. Also shown in this figure is a sample of causal light cones, depicted as circles around dots in the outer region, and inward-tilting cones inside the horizon. Reproduced from [3].

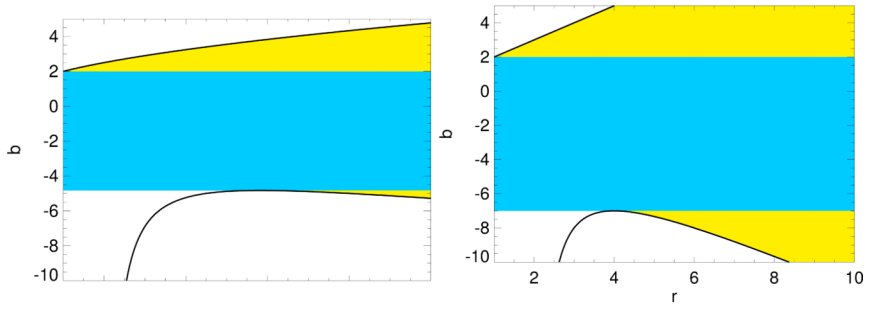

Fig. 2.

Radial turning points in the effective potential $V_{\rm eff}$ (r, b) for (*left*) massive and (*right*) massless particles, for a black hole with maximal spin $a_* = 1$. Any particle in the yellow region can escape from the black hole, but in the blue regions, only particles with outgoing radial velocities can escape. The static limit is located at $r_{\rm E} = 2$ and the horizon is at $r_+ = 1$.

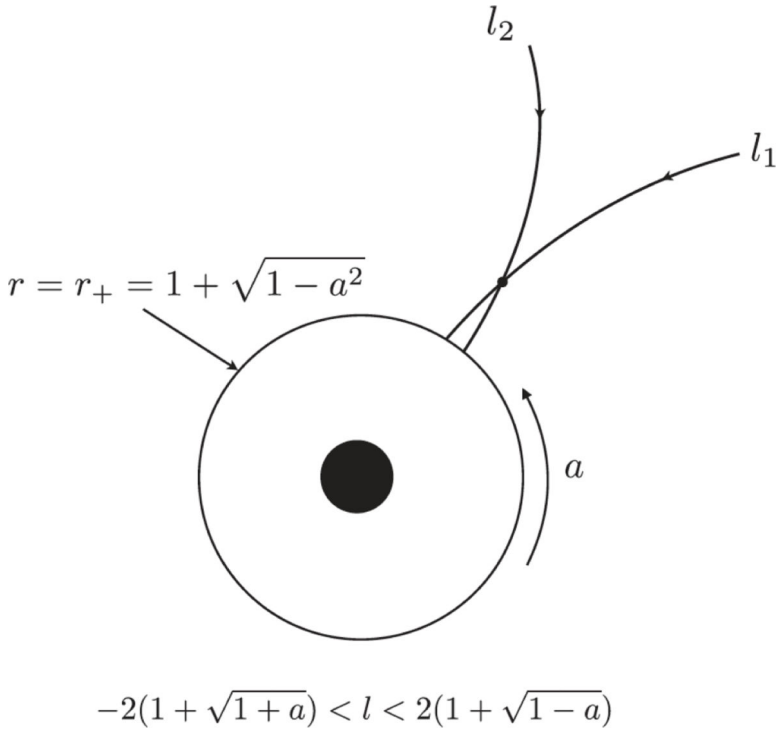

Fig. 3.

Schematic picture of two particles falling into a black hole with spin a_* and colliding near the horizon (r_+). Reproduced from [13].

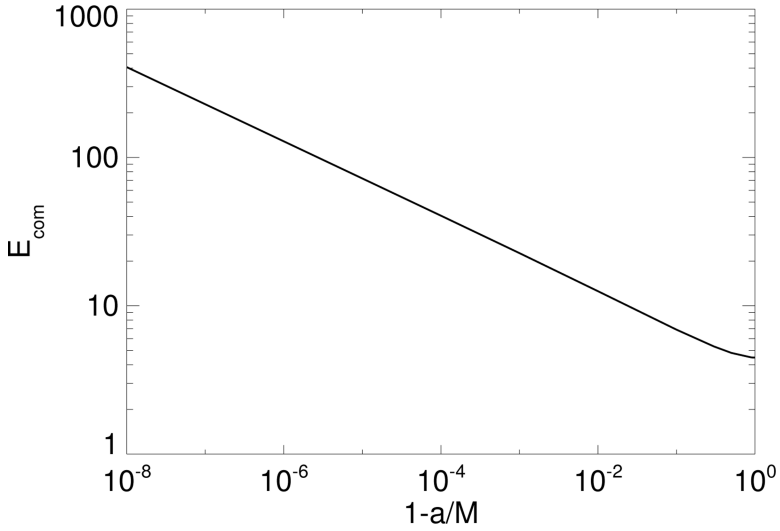

Fig. 4.

Center-of-mass energy as a function of spin for two particles falling from rest at infinity with critical impact parameters $b = \pm 2(1 + \sqrt{1 \mp a})$, colliding near the event horizon.

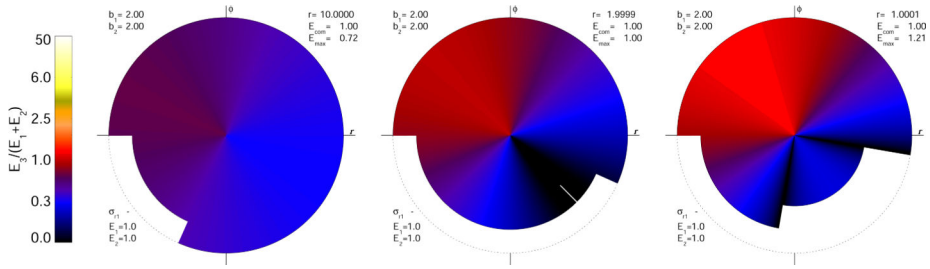

Fig. 5.

Polar plots of the energy and escape distribution of photons emitted in a classical Penrose decay process at various radii outside of an extremal Kerr black hole. The interpretation of these polar plots is described in detail in the text. The non-linear color scale represents the absolute value of the energy-at-infinity $|p_t^{(3)}|$ relative to the total input energy. $E_{\rm com}$ is the center of mass energy, normalized to the total energy of the incoming particles, and $E_{\rm max}$ is the maximum energy of the *escaping* particles, also normalized to total incoming energy.

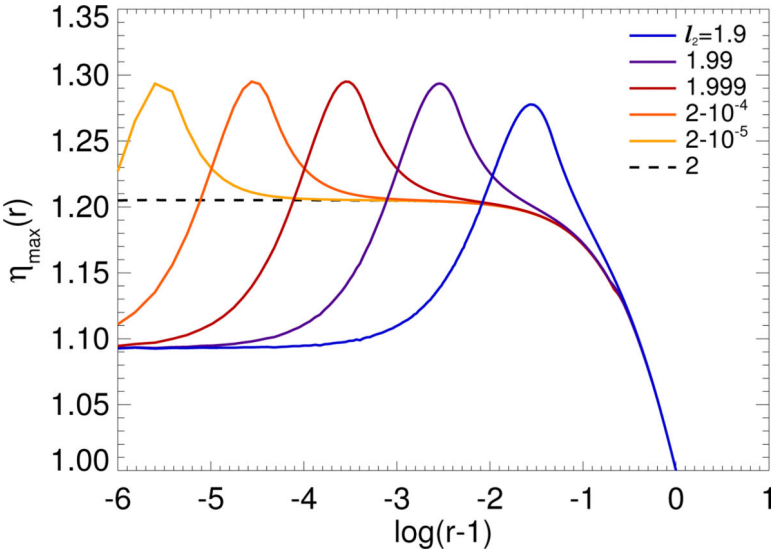

Fig. 6.

Peak efficiency for annihilation of equal-mass particles falling from rest at infinity, as a function of the radius at which the annihilation occurs. The angular momentum $b_1 = 2$ is fixed at the critical value, and b_2 varies. The black hole spin is maximal: $a = 1$. (Compare to Fig. 2 of Ref. [22])

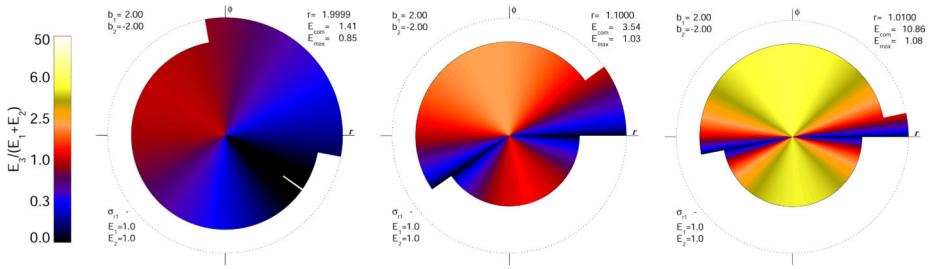

Fig. 7.

Polar plots of the energy and escape distribution of photons emitted in a Penrose annihilation reaction at various radii outside of an extremal Kerr black hole.

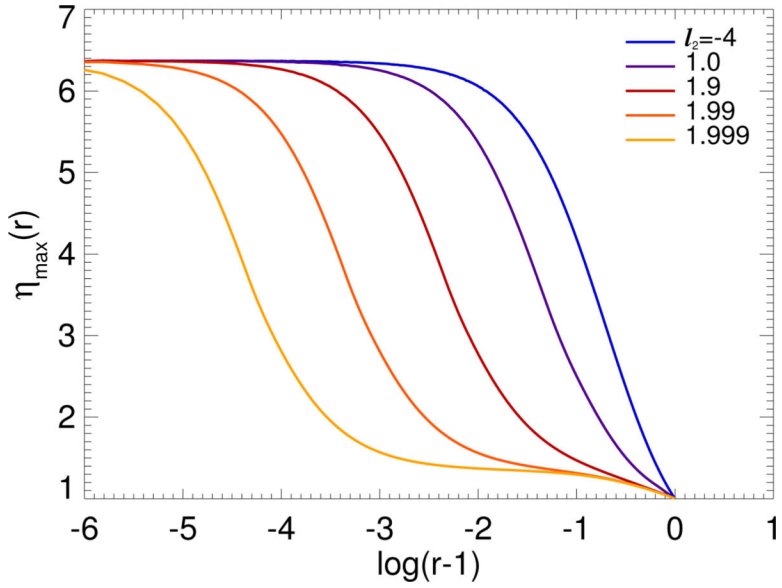

Fig. 8.

Peak efficiency for annihilation of equal-mass particles falling from rest at infinity, as a function of the radius at which the annihilation occurs. Unlike in Fig. 6, here we allow $p_r^{(1)} > 0$, which greatly increases the fraction and energy of escaping photons. The angular momentum $b_1 = 2$ is fixed at the critical value, and b_2 varies. The black hole spin is maximal: $a = 1$.

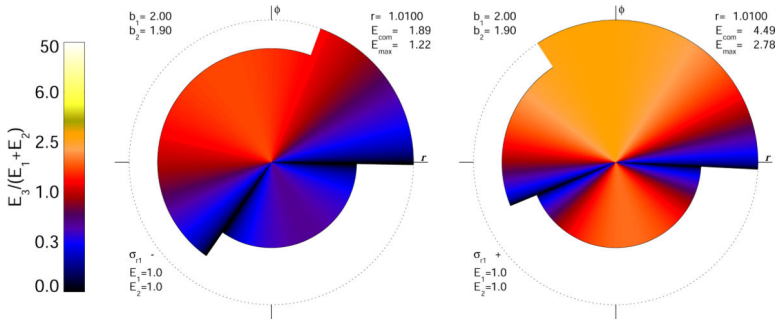

Fig. 9.

Polar plots of the energy and escape distribution of photons emitted in a Penrose annihilation reaction at $r = 1.01M$ outside of an extremal Kerr black hole. All parameters are identical, except the left-hand plot is for two ingoing particles, and the right-hand plot has an outgoing particle (1).

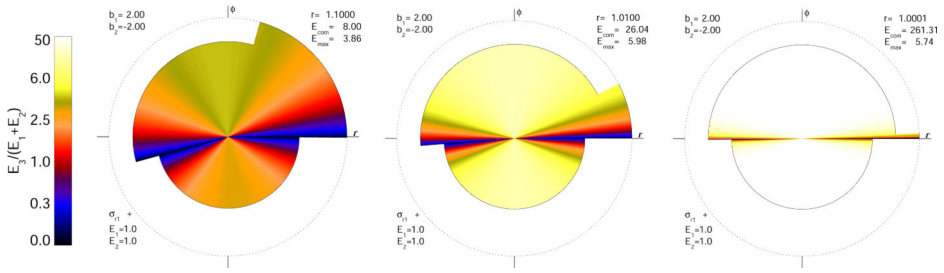

Fig. 10.

Polar plots of the energy and escape distribution of photons emitted in a Penrose annihilation reaction for nearly head-on collisions outside of an extremal Kerr black hole. As the collision radius approaches the horizon, the c.o.m. energy diverges while the escape fraction approaches zero.

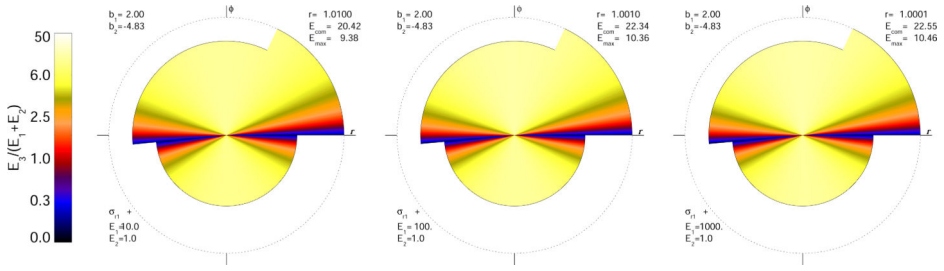

Fig. 11.

Polar plots of the energy and escape distribution of photons resulting from a Compton-like scattering event outside of an extremal Kerr black hole. The initial particles include a photon and massive particle, both falling in from infinity. As the energy of the photon increases, we need to move the position of the collision closer and closer to the horizon in order to achieve the target efficiency of 1000%.

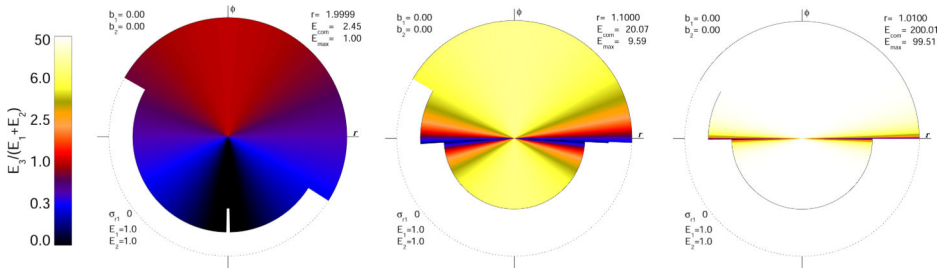

Fig. 12.

Polar plots of the energy and escape distribution of photons resulting from annihilations outside an extremal Kerr black hole.

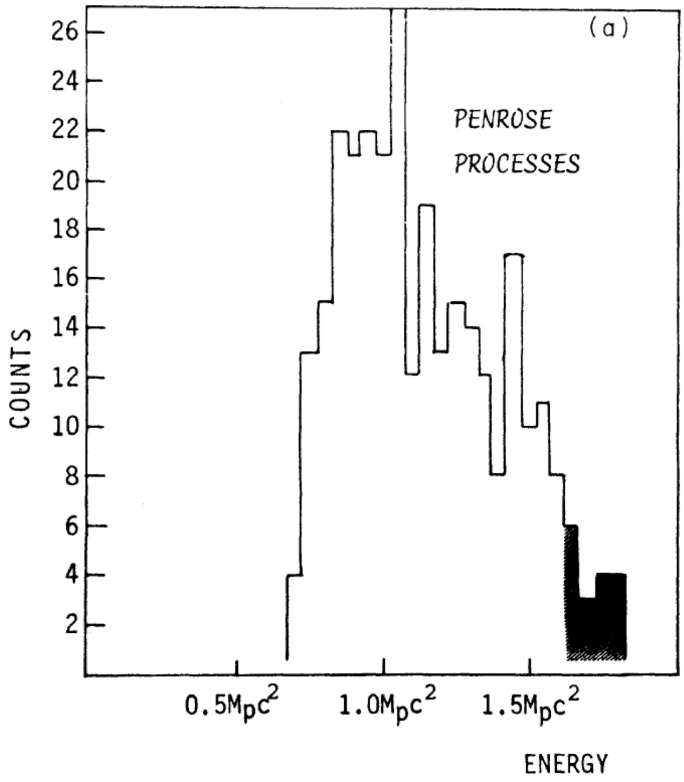

Fig. 13.

Spectrum of outgoing massive particles from a numerical scattering experiment including 1000 elastic collisions between protons with particle 1 falling in radially from infinity and particle 2 on a circular orbit at the ISCO for a black hole with spin $a_* = 0.998$. Of the 2000 protons taking place in the scattering events, only 23 escape with $E_3 > E_1 + E_2$. Reproduced from [7].

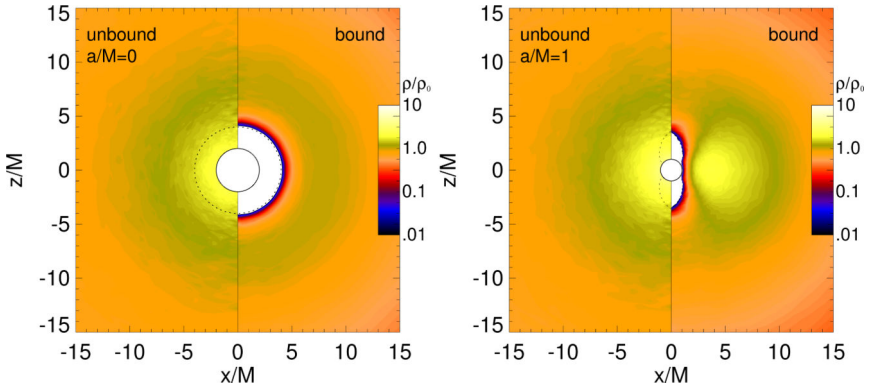

Fig. 14.

Spatial density of test particles in the $x - z$ plane, for both bound and unbound populations, for $a/M = 0$ and $a/M = 1$. For each case, we show the unbound distribution on the left side and the bound distribution on the right side of the plot, and all distribution functions are normalized to the mean density at $r = 10M$. The horizon is plotted as a solid curve and the radius of the marginally bound orbits is shown as a dotted curve. The spin axis of the black hole is in the $+z$ direction. Reproduced from [38].

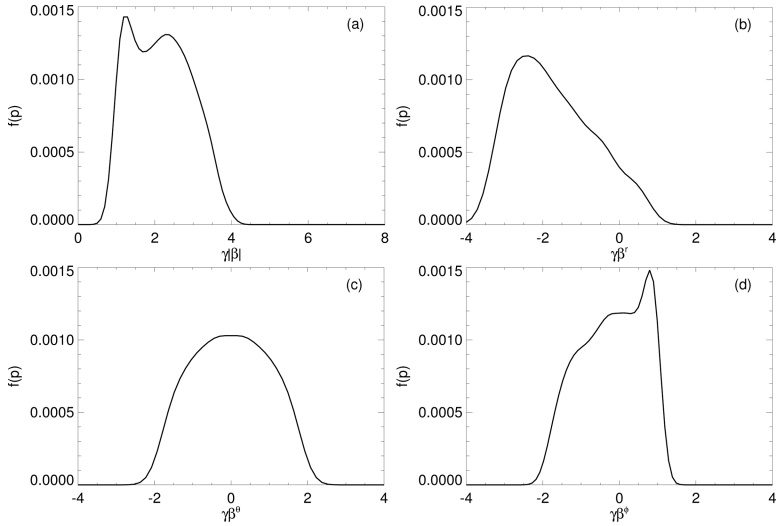

Fig. 15.

Momentum distribution of unbound particles observed by a FFIO in the equatorial plane at radius $r = 2M$. All particles have nearly unitary specific energy at infinity, so the average particle speed is on the order $\sqrt{2GM/r} \approx c$ (panel *a*). In panels (*b-d*) we show the distribution of the individual momentum components, which are decidedly non-thermal and highly anisotropic. Reproduced from [38].

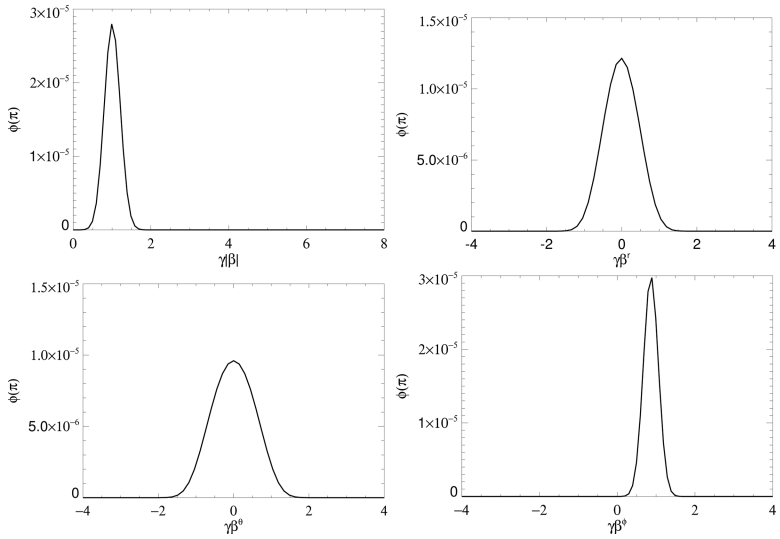

Fig. 16.

Momentum distribution of bound particles measured by a LNRF observer in the equatorial plane at radius $r = 2M$. Compared to Figure 15, here we actually see a more symmetric, thermal distribution making up a thick torus of stable, roughly circular orbits near the equatorial plane. Reproduced from [38].

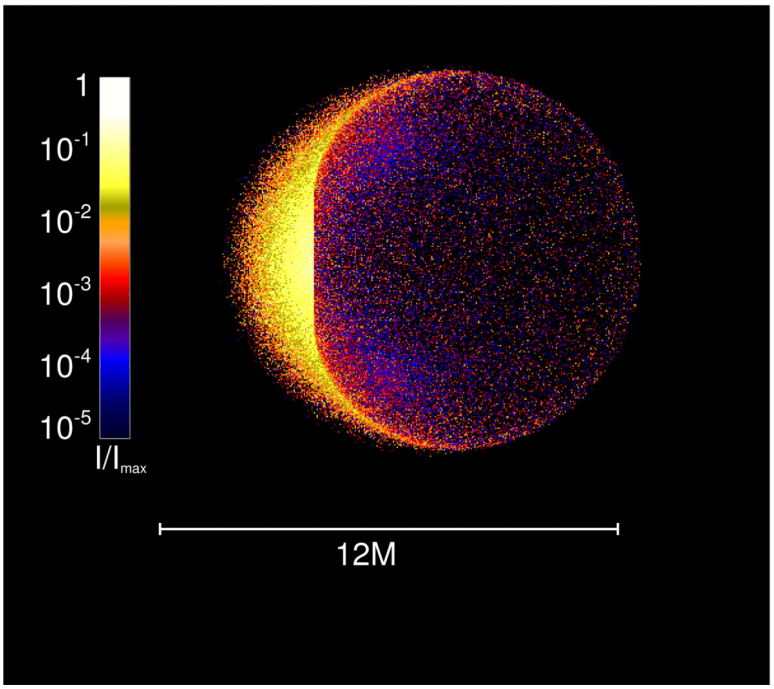

Fig. 17.

Simulated image of the annihilation signal around an extremal Kerr black hole, considering only annihilations from unbound DM particles with $E_{com} > 3m_{\chi}$. The observer is located in the equatorial plane with the spin axis pointing up. While the image appears off-centered, it is actually aligned with the coordinate origin. Reproduced from [38].

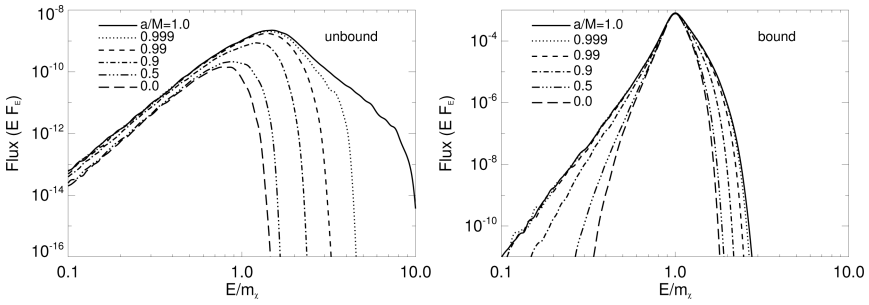

Fig. 18.

Observed flux from annihilation products near a black hole, as a function of spin parameter. (left) Contribution from the unbound population, including only annihilations with $E_{\rm com} > 3m_\chi c^2$. (right) The bound population, with $\rho \sim r^{-2}$ and no threshold energy. In all cases the observer is in the equatorial plane. The scale of the vertical axis is arbitrary. Reproduced from [38].

Table 1

Summary of results from Ref. [37], the most complete and exact work to date on maximizing energy of escaping particles ($E_{\max}$) and efficiency ($\eta_{\max}$) for the collisional Penrose process. The labeling convention for the particles is XYZsgn, with X, Y, and Z describing the properties of particles 1, 2, and 3, respectively, and 'sgn' describing the direction of the radial velocity for particle 1. 'M' refers to a massive particle falling from rest at infinity, 'P' a photon, and 'm' ('p') a massive particle (photon) with infinitessimal mass (energy) compared to its companion particle's energy. In all cases the first particle has the critical impact parameter $b_1 = 2$.

	$E_{\max}$	$\eta_{\max}$		$M_{3,\max}$	
MMP−	$2(2+\sqrt{3})$	$2+\sqrt{3}$	≈3.73		
MMP+	$(2+\sqrt{3})(2+\sqrt{2})$	$(2+\sqrt{3})(2+\sqrt{2})/2$	6.37		
PmP−	$2(2+\sqrt{3})E_1$	$2(2+\sqrt{3})$	7.46		
PmP+	$(2+\sqrt{3})^2E_1$	$(2+\sqrt{3})^2$	13.92		
MpP−	$2(2+\sqrt{3})$	$2(2+\sqrt{3})$	7.46		
MpP+	$(2+\sqrt{3})(2+\sqrt{2})$	$(2+\sqrt{3})(2+\sqrt{2})$	12.74		
MMM−	$4+\sqrt{11}$	$(4+\sqrt{11})/2$	3.66	$2\sqrt{3}$	≈ 3.46
MMM+	$7+4\sqrt{2}$	$(7+4\sqrt{2})/2$	6.32	$\sqrt{3}(2+\sqrt{2})$	5.91
PmM−	$4E_1+\sqrt{\left(12E_1^2-1\right)}$	$2(2+\sqrt{3})$	7.46	$2\sqrt{3}E_1$	$5.91E_1$
PmM+	$2(2+\sqrt{3})E_1+\sqrt{3(2+\sqrt{3})^2E_1^2-1}$	$(2+\sqrt{3})^2$	13.92	$\sqrt{3}(2+\sqrt{3})E_1$	$6.46E_1$
MpM−	$4+\sqrt{11}$	$4+\sqrt{11}$	7.32	$2\sqrt{3}$	3.46
MpM+	$7+4\sqrt{2}$	$7+4\sqrt{2}$	12.66	$\sqrt{3}(2+\sqrt{2})$	5.91